Journal of the Indian Institute of Science
A Multidisciplinary Reviews Journal
ISSN: 0970-4140 Coden-JIISAD

REVIEWS

Multi-Temporal Satellite Imagery for Flood Damage Assessment

J. Senthilnath[1], S.N. Omkar[1], V. Mani[1] and P.G. Diwakar[2]*

Abstract | Assessment of flood prone region is carried out using multi-temporal satellite imagery. The framework for precise assessment of damages caused by flood is presented using remote sensor data. We classify the framework into two categories: (1) Moderate satellite image processing using multi-temporal Moderate Resolution Imaging Spectroradiometer (MODIS) data, and (2) Optical and radar satellite image processing using Linear Imaging Self Scanning Sensor-III (LISS-III) and Synthetic Aperture Radar (SAR) data. In data set#1, spectral-spatial classification is applied on before, during and after flood MODIS imagery. As MODIS is of moderate resolution hence two classes is considered namely water and non-water region. In the case of data set#2 LISS-III (before flood) and SAR (during flood) data hierarchical classification is applied. The SAR data is used to extract flooded and non-flooded regions where as LISS III data is used to classify various land cover regions. Further, the resultant images are overlaid to analyze the extent of the flood in individual land classes. We review the major development in processing these two flood assessment frameworks.

Keywords: *multi-temporal satellite imagery, flood assessment, spectral-spatial classification, hierarchical classification.*

1 Introduction

With a rapid growth of space technology, there are varieties of satellites launched for earth observation. The major advantage of satellite technology is that the data acquired has wider scope compared to other existing technologies, since the satellite data provide a better coverage of scene in comparison to aerial data for a given location. Besides, the use of wireless technology and video surveillance need equipments to be set up in the desired region, and hence could be cost prohibitive and also be affected by various natural hazards. This problem is not encountered in the case of satellite data. Thus, the most popular and preferred means for acquiring data to monitor natural disaster—flood, earthquake and volcano eruption is satellite.

Every year floods occur in many regions of the world and cause great losses. In order to monitor and assess such situations, decision-makers need accurate knowledge of the real situation. How to provide actual information to decision-makers for flood monitoring and mitigation is an important task for public welfare. Over-estimation of the flooded area leads to over-compensation to people, while under-estimation results in production loss and negative impacts on the population. Hence there is a need for efficient flood disaster monitoring tool to endure the aftermath of flooding.[1] The most prominent tool for evaluating the flood extent is accurate analysis of multi-temporal satellite imagery.

In the assessment of flood prone region, it is necessary to create detailed land cover maps using multi-temporal satellite imagery. The multi-temporal data acquired before, during and/or after flood were used for mapping and analysis. This earth observation technique can contribute towards flood hazard modeling and can be

[1]*Department of Aerospace Engineering, Indian Institute of Science, Bangalore, India.*
[2]*Earth observation system, ISRO Head quarters, Bangalore, India.*
**omkar@aero.iisc.ernet.in*

used to assess damage to residential properties, infrastructure and agricultural crops.[2,3]

Several studies have been carried out, for example in China and throughout Europe, for monitoring of floods using multi-temporal satellite data, with encouraging results.[4] In India, some of the regions most frequently affected by floods include the Brahmaputra basin in Assam, the Kosi basin in Bihar, the Godavari basin in Andhra Pradesh, and the Yamuna basin around Delhi. The multi-temporal image features were extracted in order to compare both normal and heavy monsoon/flood conditions.

In order to develop a damage estimation framework for flood prone regions, a database using remotely sensed data (optical and microwave/Synthetic Aperture Radar data) and topographic maps can be efficiently created for certain time instant.[5,6] The spectral, spatial and contextual information are integrated, and subsequently classification is applied for extraction of flood-prone regions.

NASA's Moderate Resolution Imaging Spectroradiometer (MODIS) satellite sensor has considerable potential for applied hydrology applications such as flood detection, characterization and warning, flood disaster response and damage assessment, and flood disaster mitigation. Although MODIS is a medium-resolution image sensor (250 metre pixels) it does provide excellent land/water discrimination.[3,7] Because of the medium-resolution of MODIS, some features such as river courses, canals, and roads appear in the images as simple lines, without additional details that would further complicate the extraction of linear features.

MODIS data have attracted many researchers to work towards optical data based flood assessment because of their easy availability and cost-effectiveness. Islam et al. (2009)[8] presented a flood inundation mapping based on Normalized Difference Water Index (NDWI). Khan et al. (2011)[9] applied ISODATA algorithm for the classification of flooded and non-flooded regions using MODIS data. Sakamoto et al. (2007)[10] did an extensive research on detecting temporal changes using MODIS time-series data. Enhanced Vegetation Index and land-water surface index were employed for producing time-series inundation maps.

Optical sensors of the satellites are used to obtain data of the region prior to the flood. But such sensors are dependent on illumination by the sun, and there is also a possibility of misinterpretation of land cover map under the cloudy weather conditions.[11] However, Synthetic Aperture Radar (SAR) data have the capability of distinguishing between the land cover even during the unfavorable weather conditions because of its active sensor system which uses dipolar effect to acquire the data.[12] Hence, SAR data are used to analyze the land during flood. The optical data is classified according to the various distinct types of land cover[13] and SAR data help to determine the flooded and unflooded regions.[14]

Some of the researchers have considered both SAR (during flood) and optical data (before flood) for flood assessment. An analysis of flood inundation risks in terms of land use has been done.[15,16] Duc (2006)[15] applied Gray Level Co-occurrence Matrix (GLCM) based texture analysis and then supervised method, namely maximum likelihood classifier for flooded area segmentation. Senthilnath (2013)[16] applied speckle noise removal and image segmentation for extraction of flood affected region.

Many researchers are currently engaged in developing multi-temporal satellite image processing framework for precise assessment of damages caused by flood. In this paper, we present a survey of multi-temporal satellite image processing framework and methods for flood assessment. Our aim is to provide a better understanding of the current scenario in this field. We propose an satellite image processing framework for two scenarios: 1) to estimate accurately the flooded and non-flooded cities using MODIS data; and 2) to identify the extent and type of the inundated area using LISS-III (before flood) and SAR (during flood) data.

In literature, the aforementioned data is efficiently processed using spectral-spatial and hierarchical classification techniques. Spectral-spatial classification is applied on before, during and after flood MODIS data. MODIS is of moderate resolution, here two classes are considered for grouping (water and non-water). The river network forms a linear segment, hence, initially spectral feature method is used to classify water and non-water region. Sometimes non-water region may be misclassified as water region because of similar spectral information. To overcome this problem spatial features based on shape index and density index are also considered. In the case of LISS-III (before flood) and SAR (during flood) data hierarchical classification is applied. Here, the complex data set is split into a number of cluster centers by satisfying Bayesian Information Criteria (BIC), and the data set grouped (merged) into their respective classes. We combine the classified before and during flood data to estimate the extent of land cover affected by

the flood. The performances of aforementioned approaches are analyzed.

2 Methodology

In this section, multi-temporal satellite data is used for flood assessment using spectral-spatial classification and hierarchical classification. Some of the processing framework from the earlier works is highlighted.

2.1 *Spectral-spatial classification*

Here MODIS surface reflectance product (i.e. MOD09Q1) is used, this product contains orthorectified image. Hence co-ordinate points are sufficient to get same scene coverage for multi-temporal satellite data. So there is no need to align any of this imagery. The flow chart of the proposed approach is shown in Fig. 1. The processing steps involved are as discussed below:

2.1.1 Image restoration: Optical satellite data are often adversely affected by image "noise" due to clouds. In literature, median-based switching filter, called Progressive Switching Median Filter (PSMF), along with histogram equalization is applied to remove all the cloud noise and to enhance image quality for during flood MODIS image.[3] This is shown in Fig. 1 as preprocessing step for during flood image.

2.1.2 Image classification based on spectral features: In satellite imagery, the appearance of water strongly depends on the sensor's spectral sensitivity and its resolution. In this study, moderate-resolution grey-scale MODIS data are used. The grey-scale intensity of any pixel in an image depends on the reflectance properties of the object it depicts. Each object can therefore be classified into different groups based on its specific intensity level in the image. Due to moderate-resolution, the data is classified into two groups: water and non-water.

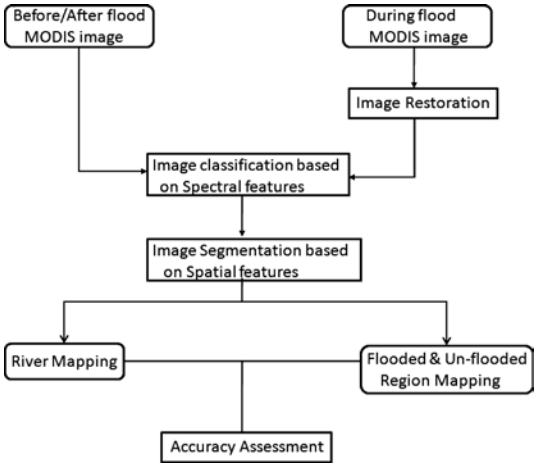

Figure 1: Flood assessment framework using MODIS data.

For our purposes, the aim of the clustering[17] is to eliminate those features which do not have the reflectance properties of water. However, as some non-water features in the image will have reflectance properties similar to water; these may be erroneously classified into the water group. Solutions are discussed in the next step. Here Genetic Algorithm is used to cluster the image using the fitness function. Senthilnath et.al (2013)[18] provide a detailed description of the problem formulation and analysis of this approach. Here, the water pixels and non-water pixels from three images (before, during and after flood) are clustered for entire image.

2.1.3 Image segmentation based on spatial features: The objective of image segmentation is to eliminate those pixels that are wrongly classified as water. However, as some non-water pixels in the image will have reflectance properties similar to water, and hence these pixels may be misclassified into the water group. Because of this, false-water pixels get classified into the true-water pixels which are a hindrance in the classification. This hindrance is removed by segmentation using spatial features of the image. The image is first divided into regions and the geometrical parameters for every region are calculated. Then these regions are segmented as true-water and false-water regions. For this we use Shape Index (SI) and Density Index (DI) defined as:[3,19]

$$SI = \frac{P}{4 \cdot \sqrt{A}} \tag{1}$$

$$DI = \frac{\sqrt{A}}{1 + \sqrt{VAR(X) + VAR(Y)}} \tag{2}$$

where P represents the perimeter of the region (the number of pixels on the boundary of the region), A represents the area of the region (the number of pixels of the region), $VAR(X)$ represents variance of x-coordinates of all the pixels in the region, $VAR(Y)$ represents variance of y-coordinates of all the pixels in the region and the term $\sqrt{VAR(X)+VAR(Y)}$ gives an approximate radius of the region.[3,19]

The river pixels have a high SI and a low DI, whereas non-river pixels have a low SI and a high DI.

Thus, for segmentation purpose, threshold values are set for both indices: SI and DI. Regions having a SI greater than the SI threshold value, and a DI lower than the DI threshold value, are segmented as water and non-water regions. Those regions which do not qualify as water are segmented as non-water. We see that the non-flooded regions (false-water) are more than the flooded region in an image. The perimeter value of a non-flood region is greater than that of a flood region. This makes the ratio of perimeter to the area, a high value for non-flood region and a low value for flood region. Thus, non-flood regions have a higher value of SI than flood regions, and hence, the DI for flooded regions is higher than that for non-flooded regions. Thus, for segmenting purpose, threshold values can be set for both the indices: SI and DI. Regions having a SI lower than the threshold value and DI higher than the threshold value are segmented as flooded regions.

2.1.4 Accuracy assessment: The performance of image clustering and segmentation algorithm is evaluated using Root Mean Square Error (RMSE)[3,18] and Region of Convergence (ROC)[3,18] methods.

2.2 *Hierarchical classification*

Here flood damage assessment using multi-sensor data is carried out using LISS-III (before flood) and SAR (during flood). The flow chart of the proposed approach is shown in Fig. 2. The processing steps involved are as discussed below:

2.2.1 Speckle removal filter: Gamma MAP filter is based on the Bayesian analysis of image statistics. It uses the Maximum A-Posteriori (MAP) estimation method. While using this filter, Gamma distribution is assumed for the underlying image and the speckle noise in it. Thus this filter works best for geo-spatial images containing homogenous areas such as oceans, forests and fields.[20]

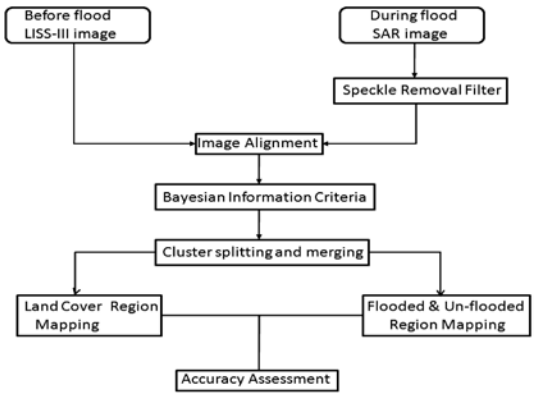

Figure 2: Flood assessment framework using LISS-III and SAR data.

2.2.2 Image alignment: The task of image alignment involves establishment of correspondence between LISS-III and SAR data. Image alignment[21] is an essential step for geometrically aligning an image obtained from different sensors, different times, or from different viewpoints with a reference (LISS-III) image. This image which is aligned is called the sensed (SAR) image, and the image with respect to which alignment is carried out is called the reference (LISS-III) image. The transformed sensed image which aligns with the reference image is called the registered (SAR) image.

Image alignment involves feature detection, matching and transformation. Also in comparison with before flood (LISS-III) image, during flood (SAR) image there may be scene changes and growth due to inundated regions, this is taken care in this step.

Here, feature detection (keypoints) is carried out on LISS-III and SAR data using Scale Invariant Feature Transform (SIFT)[22] and these keypoints matching is employed based on objective switching Genetic Algorithm (GA). This approach was proposed by Senthilnath et.al (2012)[23] and this paper provides a detailed description of the problem formulation and analysis of this approach. From these matched keypoints, the SAR image can be registered using the affine transformation which takes into account scaling, shearing, rotation and translation.

2.2.3 Bayesian information criteria: For large data sets, it is difficult to determine the number of clusters required, as it depends on the distribution of the given data. A platform is needed, from where an optimal number of cluster centers can be picked for a given data set. Bayesian Information Criteria (BIC)[24] is a model fitting approach, which provides the optimal number of clusters. The splitting of data set using BIC[24,25] into number of clusters is given by

$$BIC = L(\theta) - 0.5 * k_j * \log(n) \quad (3)$$

where $L(\theta)$ is the log-likelihood measure for the data set, k_j is the number of free parameters for the specific number of clusters and n is the number of data points for a given data set.

2.2.4 Cluster splitting and merging: The cluster analysis forms the assignment of data set into clusters based on some similarity measure. In this

study, cluster splitting using Niche Genetic Algorithm (NGA)[6] and merging method using voting technique[6] is applied. These hierarchical splitting techniques make use of kernel functions for locating maxima for a given set of discrete data points.

After obtaining cluster centers from NGA, data points are merged to its closest cluster centre. Grouping the data points to exact number of class is done using voting methodology. In voting method classification of clusters is done using class labels. If the majority of the data points belong to a particular class then the whole cluster is labeled as that class. In some cases, if the number of data points of a class is less, then majority voting fails. To overcome this ambiguity a threshold is set for class having less data points.[6]

2.2.5 Accuracy assessment: The performance of hierarchical classification is evaluated using producer's accuracy (PA), user's accuracy (UA), overall accuracy (OA) and Kappa coefficient.[25,26]

3 Result and Discussions

In this section, we present the flood assessment using spectral-spatial classification for MODIS data and hierarchical classification for LISS-III and SAR data.

3.1 *Data set#1: MODIS imagery*

Region surrounding Krishna river near Manthralaya, Andhra Pradesh is taken as study area. The dataset obtained from MODIS (MOD09Q1) Terra surface reflectance 8-Day L3 Global 250 m^2 satellite images are used for this purpose. This dataset comprises 2 bands. Band 1 (visible red region) lies between 620–670 mm and Band 2 (Near Infra-Red region) is centred between 841–876 mm. Band 1 is more sensitive for the detection of land/cloud boundaries while NIR band is more efficient in detecting water region since water has significant low reflectance in NIR region.[3,7]

All the MODIS data are clustered into two classes (water and non-water) using Genetic Algorithm (GA).[18] The pixels are eventually clustered as water and non-water region. In GA, crossover operator tries to optimize the solution globally while the mutation operator searches locally. So we use the variable rates of crossover and mutation to aid swift optimization. The chromosome with best fitness value is used to cluster the image. The clustering result of the Krishna River before and after flood (i.e. March 2009 and November 2009) by the GA technique is shown in Figs. 3(b) and 4(b).

The failure of classification to extract water features from the images is overcome by segmen-

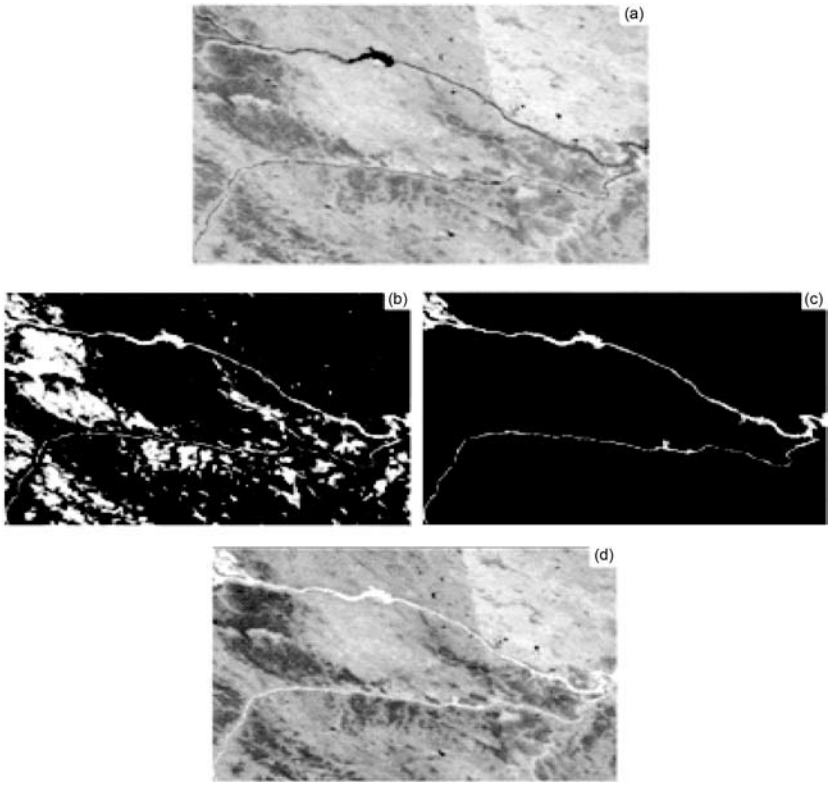

Figure 3: (a) MODIS image of Krishna river before flood (b) Image clustering using GA (c) Segmented image (d) River mapping of segments of GA classified image shown on backdrop of original image.

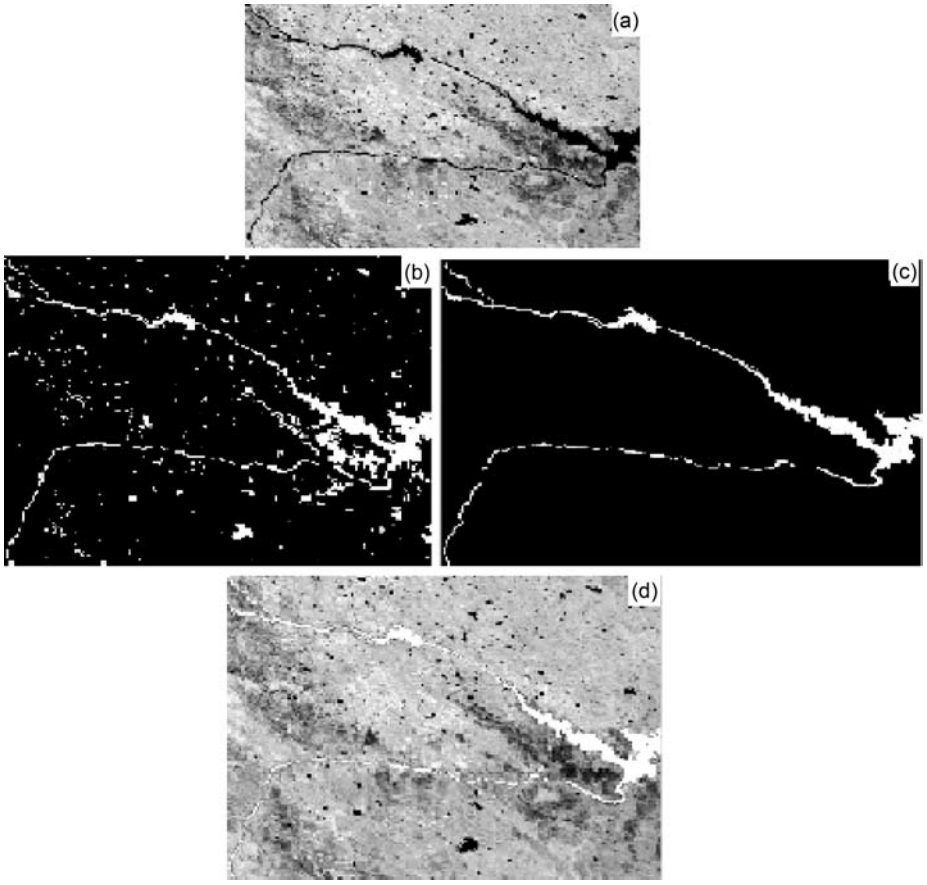

Figure 4: (a) MODIS image of Krishna river before flood (b) Image clustering using GA (c) Segmented image (d) River mapping of segments of GA classified image shown on backdrop of original image.

tation. For segmentation purpose, we use the spatial, i.e. geometrical features of the linear segments. We use two indices as geometrical features—Shape Index (SI) and Density Index (DI). Using these, the linear segments are differentiated from non-linear segments by thresholding values of these indexes.

From Figs. 3(c) and 4(c) we can observe that segmentation eventually extracts the linear features from images to a reliable extent. In case of image of Krishna river system before and after flood, the final segmented images as a result of classification by GA are shown on a backdrop of the original image in Figs. 3(d) and 4(d). In these images, river course is represented by white pixels. It has been observed that RMSE value for GA with segmentation for before and during flood image is 0.18 and 0.16 respectively.

To assess the quality of extraction of flood area in image of Krishna river image during the flood, i.e. September 2009, a list of cities situated in the flooded region is created. To create this list, all the cities situated in the region shown in the image were plotted on the original image as points as shown in the Fig. 5(a). The cities which were not affected by flood are represented by white discs whereas affected cities are represented by white discs with black dots in the center.

The cities flooded, according to classification by GA, are shown as white dots in the Fig. 5(b). The result of Fig. 5(b) is evaluated using the terms like True Positive (TP), False Positive (FP), True Negative (TN) and False Negative (FN). These ROC parameters are TPA, TNR, FPR and ACC. Total number of cities flooded is 12 and GA has identified 10 cities, and 2 places is misclassified; from 16 non-flooded places it has picked 15 correctly and 1 place is misclassified. From this measure, we can obtain ROC parameters: true positive rate is 0.83, true negative rate is 0.94, false positive rate is 0.06 and accuracy is 0.89.

In literature, the methods such as k-means[27] and Mean Shift Segmentation (MSS)[28] are widely used for image segmentation. In our study, we applied these methods to segment before flood (March 2009) image.

From these two methods, we can observe that RMSE value for k-means is 0.45 and MSS is 0.26.

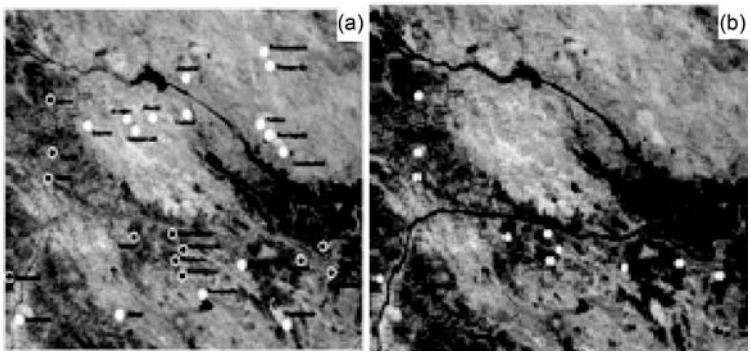

Figure 5: (a) MODIS during flood image with ground truth information—flooded (white discs) and non-flooded cities (black discs at the centre) (b) Segmented image using GA (White pts. are flooded cities).

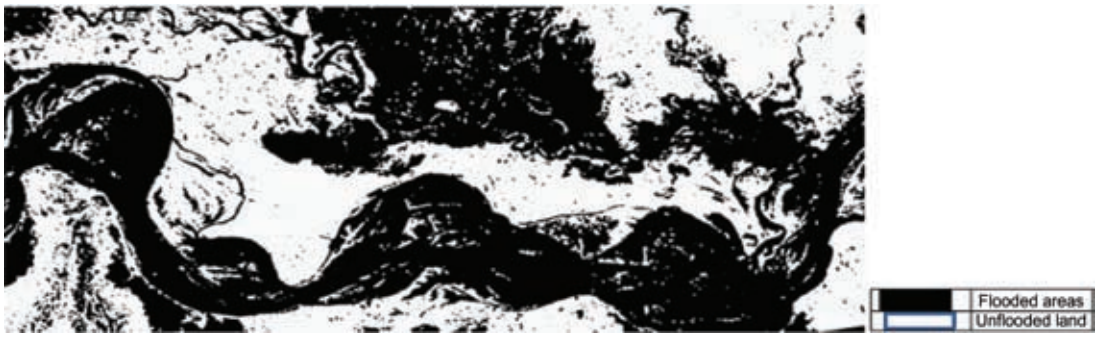

Figure 6: SAR image classification using NGA.

In comparison, with these methods RMSE value of GA is 0.18 which is better than k-means and MSS.

3.2 *Data set#2: LISS-III and SAR data*

The study area includes the regions affected by the Kosi river flood in Bihar during 2008. We focused mainly on the Bhagalpur district, where the Kosi tributary merges with Ganges, and assess the extent of damage caused. The districts affected by the flood and covered in this image include Bhagalpur, Khagaria, Katihar and Madhepur.

We use LISS-III image to assess the land cover prior to the flood. It was collected on April 11, 2008 from RESOURCESAT-2. For flood delineation, we use SAR *C*-band dataset obtained from RADARSAT-2 on August 27, 2008 during the flood. The spatial resolution of the LISS-III image is 23.5 meters per pixel and SAR image is 30 meters per pixel. The image dataset used is of size 1614×3645 pixels. The SAR image is separated into two classes, namely flooded and non-flooded. The LISS-III image is classified into 4 different land cover types, namely urban land, fallow land, water and vegetation. Initially, speckle removal is done on the SAR image by applying Gamma-MAP filter and SAR image is aligned using LISS-III image.[16,23] For these data BIC is applied to determine the optimal number of clusters required for the data. We observe that the optimal number of clusters is 9 for SAR image and 100 for LISS-III image.

We apply ISODATA[29] and Niche Genetic Algorithm (NGA)[6] to generate 9 number of clusters, as specified by BIC on SAR image. We then merge them into 2 classes, corresponding to flooded (A_1) and unflooded region (A_2). The resultant image using NGA is shown in Fig. 6. We compare the performance of these techniques in classifying the SAR image, and the results are tabulated in Table 1. From this table, we observe that the two techniques managed to effectively pick all the flooded and unflooded regions, although some portion of flooded region has been incorrectly classified as unflooded. This is caused by the change in the dielectric value of the inundated surface, which thus appears unflooded. NGA gives marginally better results, both in terms of overall accuracy and Kappa coefficient.

We apply ISODATA and Niche Genetic Algorithm (NGA) to generate 100 number of clusters, as specified by BIC on SAR image. Further, we merge them into 4 classes, namely urban land (B_1), fallow land (B_2), water (B_3) and vegetation (B_4). The resultant image using NGA is shown in Fig. 7.

Table 1: Comparison of classification performance on SAR image.

	ISODATA		NGA	
	Producer accuracy	User accuracy	Producer accuracy	User accuracy
A_1	84.37	98.31	92.60	95.16
A_2	97.91	81.33	93.23	89.75
Overall Accuracy	89.93		92.86	
Kappa Coefficient	0.7981		0.8533	

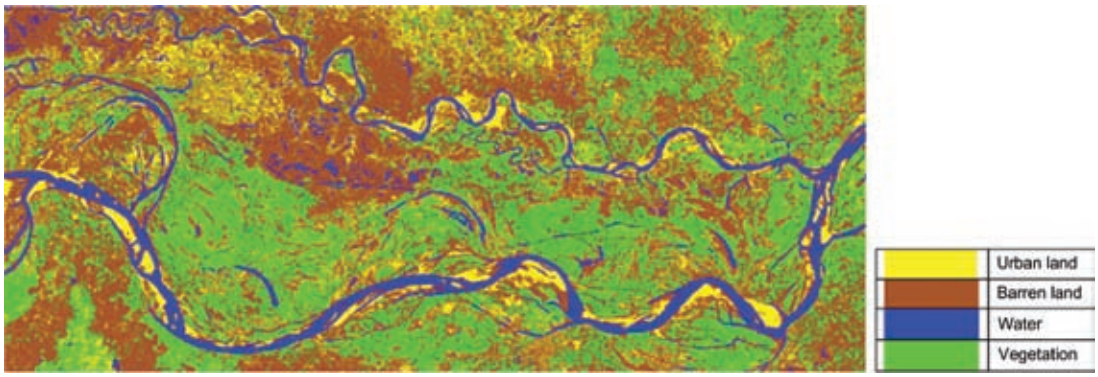

Figure 7: LISS-III image classification using NGA.

Table 2: Comparison of classification performance on LISS-III image.

	ISODATA		NGA	
	Producer accuracy	User accuracy	Producer accuracy	User accuracy
B_1	26.09	14.04	51.15	36.67
B_2	77.67	74.57	85.55	85.45
B_3	66.41	87.80	90.61	81.51
B_4	45.76	52.64	70.56	77.64
Overall Accuracy	67.23		81.22	
Kappa Coefficient	0.3668		0.6451	

We compare the performance of these techniques in classifying the LISS-III image, and the results are tabulated in Table 2. We observe that NGA provides far superior results in comparison with the ISODATA. In all the techniques, the accuracy is low for the class having less data points, namely class B_1, which represents urban region. Since we use hierarchical clustering, the cluster centers of these smaller classes are not picked, and the points get misclassified into the larger classes. The user accuracy for class B_1 is poor for ISODATA, but NGA has picked it with greater accuracy.

Further, the classified data of LISS-III and that of SAR, obtained using ISODATA and NGA, are overlaid, to obtain the resultant image that gives the flood extent in each class of the LISS-III image. It consists of 7 classes, namely unflooded urban land (C_1), unflooded fallow land (C_2), water (C_3), unflooded vegetation (C_4), flooded urban land (C_5), flooded fallow land (C_6) and flooded vegetation (C_7). Further, the image obtained by overlaying the results of NGA on LISS-III and SAR images, is shown in Fig. 8.

We compare the results of the techniques in terms of accuracy of the overlaid image,[30] and the results are tabulated in Table 3. Here we have 7 classes, corresponding to the flooded and unflooded portions of the land cover types. We observe that the flooded portion of a particular land class tends to get misclassified to its corresponding unflooded class. Also, the classes having less data points, namely class C_1 and C_5 corresponding to

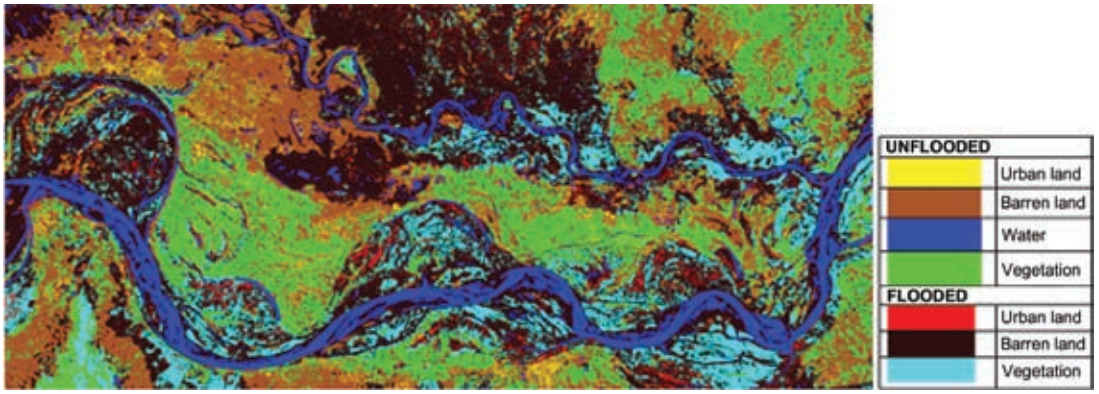

Figure 8: Overlaid image of SAR and LISS-III images using NGA.

Table 3: Comparison of classification performance on overlaid image.

	ISODATA		NGA	
	Producer accuracy	User accuracy	Producer accuracy	User accuracy
C_1	24.29	11.39	56.95	33.41
C_2	72.99	58.33	79.27	74.70
C_3	66.41	87.80	90.61	81.51
C_4	47.04	47.16	65.47	73.28
C_5	23.11	13.69	42.83	35.67
C_6	67.23	74.95	79.56	82.89
C_7	33.66	47.00	63.68	68.68
Overall Accuracy	60.82		75.78	
Kappa Coefficient	0.4807		0.6794	

unflooded and flooded urban regions, tend to get misclassified into different land cover types. This is because their cluster centers are not picked, and get merged with the larger classes. NGA provides more optimal results, and picks all the classes with greater accuracy than ISODATA.

4 Conclusions

Multi-temporal time series analyses of satellite images are useful for specific applications. Applications include, but are not limited to, agriculture mapping, flood assessment, fuel type assessment and soil moisture mapping. Here a survey on multi-temporal satellite data for flood assessment is presented. This is very valuable for the decision makers who plan for flood management measures.

We have surveyed in this paper issues on two different categories: (1) Moderate satellite image processing framework, and (2) Optical and Radar satellite image processing framework. We have summarized and compared different processing methods. We have presented the spectral-spatial classification using MODIS (before, during and after) flood data and hierarchical classification using LISS-III (before flood) and SAR (during flood) data for assessment of flood prone region. Moreover, we have highlighted improvements and research in each satellite image processing techniques on aforementioned data set.

Acknowledgment

The authors would like to thank the reviewer for their comments that helped in improving this paper.

We would like to thank NASA, USA for providing MODIS data, ISRO, India, for providing LISS-III data and CSA, Canada for providing SAR data.

We also like to thank Ashoka Vanjare, Ritwik Rajendra, Shreyas P.B, Vikram Shenoy H, Ram Prasad, C.S. Arvind and Shivesh Bajpai for valuable input in this study.

Received 20 February 2013.

References

1. Walkey J A, Development of a change detection tool for image analysis, *MS thesis, University of Wisconsin-Madison*, 1997.
2. Shaker A, Yan W Y, Wong M S, Nagwa E and Bahaaeddin I A, Flood hazard assessment using panchromatic satellite imagery, *The International Archives of the Photogrammetry Remote Sensing and Spatial Information Sciences. Vol. XXXVII*, Beijing, 2008.
3. Senthilnath J, Shivesh B, Omkar S N, Diwakar P G and Mani V, An approach to Multi-temporal MODIS Image analysis using Image classification and segmentation, *Advances in Space Research,* 50(9), (2012) 1274–1287.
4. Veronique P, Zhou Z and Songde M A, A Framework for flood assessment using satellite images, *In: Geoscience and Remote Sensing IGARSS. IEEE International*, (1998) 822–824.
5. Wang S, Liu Y, Zhou Y and Wei C, Study on the method of establishment of normal water extent database for flood monitoring using remote sensing, *In: Geoscience and Remote Sensing. IGARSS. IEEE International.* (2002) 2048–2050.
6. Senthilnath J, Shreyas P B, Ritwik R, Omkar S N, Mani V and Diwakar P G, Multi-Sensor Satellite Image Analysis using Niche Genetic Algorithm for Flood Assessment, *Swarm, Evolutionary and Memtic Computing Conference, (Eds. B.K. Panigrahi et al.) Springer-Verlag Berlin Heidelberg, LNCS 7677,* (2012) 49–56.
7. Brakenridge R and Anderson E, MODIS-based flood detection, mapping and measurement: the potential for operational hydrological applications, *in: Transboundary Floods: Reducing Risks Through Flood Management. Springer-Verlag*, (2006) 1–12.
8. Islam A K, Bala, S K and Haque A, Flood inundation map of Bangladesh using MODIS surface reflectance data, *2nd Intl. Conf. on Water and Flood Management*, 2009.
9. Khan S I, Hong Y, Wang J, Yilmaz K K, Gourley J J, Adler R F, Brakenridge G R, Policelli F, Habib S and Irwin D, Satellite remote sensing and hydrologic modelling for flood inundation mapping in lake Victoria Basin: Implications for hydrologic prediction in ungauged basins, *IEEE Tran.on Geoscience and Remote Sensing*, 49, (2011) 85–95.
10. Sakamoto T, Nguyen N V, Kotera A, Ohno H, Ishitsuka N and Yokozawa M, Detecting temporal changes in the extent of annual flooding within the Cambodia and the Vietnamese Mekong Delta from MODIS time-series imagery, Remote sensing of environment, 109(3), (2007) 295–313.
11. Zhou C H, Luo J C, Yang C J, Li B L and Wang S L, Flood monitoring using multitemporal AVHRR and RADARSAT imagery, *Photogrammetric Engineering and Remote Sensing,* 66(5), (2000) 633–638.
12. Freeman A and Durden S, A three component scattering model for polarimetric SAR data, *IEEE Tran. of Geoscience and Remote Sens.*, (1998) 36963–36973.
13. Shamaoma H, Kerle N and Alkema D, Extraction of flood-modelling related base-data from multi-source remote sensing imagery, *In: ISPRS Mid-Term Symp. Remote Sens.: From Pixels to Processes, ITC, Enschede* (2006).
14. Nataliia K, Andrii S and Serhiy S, Intelligent computations for flood monitoring, *14th Int. Conf. of Knowledge-Dialogue-Solution, Varna, Bulgaria*, (2008) 48–54.
15. Duc V B, Advantage of the remote sensing data utilization in studying inundation risks in terms of land-use, *IEEE Int. Conf. on Geoscience and Rem. Sen. Symp.,* (2006) 279–282.
16. Senthilnath J, Vikram S H, Ritwik R, Omkar S N, Mani V and Diwakar P G, "Integration of speckle de-noising and image segmentation using Synthetic Aperture Radar image for flood extent extraction", *Journal of Earth System Science, (Springer-Verlag)*, In Press.
17. Senthilnath J, Omkar S N and Mani V, Clustering using firefly algorithm: performance study, *Swarm and Evolutionary Computation*, 1(3), (2011) 164–171.
18. Senthilnath J, Vikram S H, Omkar S N and Mani V, Spectral-spatial MODIS image analysis using Swarm intelligence algorithms and region based segmentation for flood assessment, *Proceedings of Seventh International Conference on Bio-Inspired Computing: Theories and Application (BIC-TA 2012), (Eds. J.C. Bansal et al.), Advances in Intelligent Systems and Computing,* 202, (2013) 163–174.
19. Mingjun S and Daniel C, Road Extraction Using SVM and Image Segmentation, *Photogrammetric Engineering & Remote Sensing,* 70(12), (2004) 1365–1371.
20. Lopes A, Nezry E, Touzi R and Laur H, Maximum A Posteriori Speckle Filtering and First Order texture Models in SAR Images, *10th Ann. Int. Symp. on Geosci. and Rem. Sen.,* (1990) 2409–2412.
21. Senthilnath J, Omkar S N, Mani V and Karthikeyan T, Multi-objective Discrete Particle Swarm Optimization for Multi-sensor Image Alignment, *IEEE Geoscience and Remote Sensing Letters (GRSL)*, *In Press*.
22. Lowe D G, Distinctive image features from scale-invariant key-points, *International Journal of computer vision* 60, (2004) 91–110.
23. Senthilnath J, Omkar S N, Mani V, Naveen P K and Diwakar P G, Multi-objective genetic algorithm for efficient point matching in multi-sensor satellite image, *in the Proceedings of the IEEE International Geoscience and Remote Sensing Symposium,* (2012) 1761–1764.
24. Schwarz G, Estimating the dimension of a model, *The Annals of Statistics,* 6(2), (1978) 461–464.
25. Senthilnath J, Omkar S N, Mani V, Tejovanth N, Diwakar P G and Archana S B, Hierarchical Clustering Algorithm for Land Cover Mapping using Satellite Images, *IEEE Journal of Selected Topics in Applied Earth Observations and Remote Sensing (IJSTARS)*, 5(3), (2012) 762–768.

26. Senthilnath J, Omkar S N, Mani V, Nitin K and Shreyas P B, Crop stage classification of hyperspectral data using unsupervised techniques, *IEEE Journal of Selected Topics in Applied Earth Observations and Remote Sensing (IJSTARS)*, In Press.
27. MacQueen J, Some methods for classification and analysis of multivariate observations, *in Proc. 5th Berkeley Symp.,* (1967) 281–297.
28. Comaniciu D and Meer P, Mean shift: A robust approach toward feature space analysis, IEEE Trans. Pattern Anal. Mach. Intell., 24(5), (2002) 603–619.
29. Ball G H and Hall D J, ISODATA A novel method of data analysis and pattern classification, *Menlo Park: Stanford Research Institute (NTIS No. AD 699616)*, 1965.
30. Senthilnath J, Rajeswari M and Omkar S N, Automatic road extraction using high resolution satellite image based on texture progressive analysis and normalized cut method, Journal of the Indian Society of Remote Sensing, 37(3), (2009) 351–361.

J. Senthilnath is a research scholar at the Department of Aerospace Engineering, Indian Institute of Science, Bangalore, India. His research interests include nature inspired computational techniques, remote sensing, image analysis, soft computing techniques in natural hazards, and machine learning.

V. Mani is a professor at the Department of Aerospace Engineering, Indian Institute of Science. Bangalore. His research interests include distributed computing, queuing networks, evolutionary computing, neural computing, and mathematical modeling. He is a coauthor of a book, Scheduling divisible loads in parallel and distributed systems (Los Alamitos, CA: IEEE Computer Society Press).

S.N. Omkar is a principal research scientist at the Department of Aerospace Engineering, Indian Institute of Science, Bangalore, India. His research interests include nature inspired computational techniques, satellite image processing, and parallel computing.

P.G. Diwakar is a Director Earth Observation System, ISRO, Bangalore, India. His research interests include digital image processing, geospatial technologies, software and system design, and societal applications of space technology.